Improving Ranging with Analog Wi-Fi Radios: Methods and Analysis

Ian Sharp[1], Kegen Yu[2]

[1]Formerly with CSIRO ICT Centre, 25 Wyuna Road, West Pymble, NSW 2073, Australia

[2]Australian Centre for Space Engineering Research, University of New South Wales, Sydney, NSW 2052, Australia

[1]isharp25@optusnet.com.au; [2]kegen.yu@unsw.edu.au

Abstract

This paper presents techniques and analysis of time-of-arrival (TOA) based ranging with analog chip-radios used for IEEE 802.11 (Wi-Fi). TOA and round-trip-time estimation, reconstruction of a wideband signal, and local oscillator clock frequency-offset estimation are addressed. Theoretical performance analysis is performed and concise formulas are derived. Both the theoretical and experimental results demonstrate that by means of these techniques it is feasible to achieve sub-meter ranging accuracy in severe non-line-of-sight (NLOS) indoor environments using the same analog chip radios as used for Wi-Fi data communications.

Keywords

Wi-Fi Chip Radios; Time-of-arrival; Round-trip-time Ranging; Frequency Offset Determination; Wideband Signal Reconstruction; Performance Analysis; Experimental Verification

Introduction

The development of mobile radio systems has been dramatic, partly due to the development of chip radio systems, including both the analog radio transmitter and receiver. Initially, hardware was based on both analog radio chips and a separate digital signal processing chip, but later versions integrated both these functions into a single chip. While the main focus of these developments has been on digital radio communications, in more recent times the availability of integrated single chip Global Positioning System (GPS) receivers (Samper *et al* 2009, Diggelen 2009) has allowed the rapid development of position-based services in devices such as "smart" phones. Simultaneously, radio technology has been extended to indoor environments for wireless data communications, particularly the widespread adoption of IEEE 802.11 (Wi-Fi) as the defacto standard. With the availability of integrated chips, Wi-Fi has become standard in both Notebook/Tablet computers and in smart phones, with Wi-Fi base stations for data communications currently common in both workplace and home. Investigations on Wi-Fi positioning started more than one decade ago and since then Wi-Fi positioning has drawn significant attention mainly due to its simplicity. For instance, it has been used in commercial applications such as tracking mobile phones indoors when the GPS fails to work. However, accurate (say better than 1 meter) radiolocation is not commonly available, although applications such as tracking people (security, first responder/emergency and sporting applications) and assets (Bahl & Padmanabhan 200, Fontana *et al* 2003, Fontana 2004, Hedley *et al* 2008, Mourad *et al* 2011) are commonly cited as future developments with such accuracy as a requirement.

In indoor environments GPS may not work well since the satellite signals are blocked by the buildings, and typically non-line-of-sight (NLOS) multipath conditions predominate. Accuracy requirements for dense urban environments and indoor locations are typically much greater than the corresponding requirements for outdoor positioning. For example GPS accuracy outdoors is typically around 10 meters (Diggelen 2009), while for the indoor case with applications such as tracking people, an accuracy of 1 meter or better is desirable to allow location determination, such as to a particular room inside a building. Although GPS repeaters may be used to obtain better performance (Jardak & Samama 2009), in general GPS cannot meet these operational requirements indoors, and thus some other technology is required. This paper investigates the possibility that the chip radio used for Wi-Fi data communications could also be used for indoor position determination with 1-meter accuracy.

Because of the complexity of the indoor radio propagation environment, it is difficult to achieve 1-meter radio ranging accuracy. While UWB systems can have good indoor ranging error performance of the order of 10-20 centimeters, the severe limitation on the available transmitter power restricts the range to typically 10 meters (Roy *et al* 2004, Ghassemzadehl *et al* 2005,

Alavi & Pahlavan 2006, Bellusci *et al* 2008, Gentile & Kik 2006, Alsindi *et al* 2009). Thus, to cover large indoor spaces, a large number of nodes is required, which is logistically difficult and expensive. An alternative is to use the industrial, scientific and medical (ISM) bands (particularly the 2.4 GHz and 5.8 GHz bands) as used by Wi-Fi devices, where the much higher allowable transmitter power (FCC Part 15) results in indoor ranges of typically 40-80 meters, and hence far fewer nodes are required to cover the same area. However, with maximum bandwidths of respectively 80 MHz and 150 MHz, the time resolution of ISM-band positioning systems is much less than that of UWB systems, and the positional accuracy is considerable worse (Yu *et al* 2009). While the development of specific new technologies may meet future needs, a commercially attractive alternative is to adapt the current Wi-Fi data communications technology for high-accuracy radiolocation. It is noted that the 20 MHz Wi-Fi channel bandwidth will have a nominal time resolution (pulse rise-time) of the order of 100 ns (or about 30 m), but the actual ranging accuracy depends on many other factors including the operating environment (outdoors/indoors), signal-to-noise ratio, quality of the analog radio hardware, and the signal processing algorithms. Section 2 provides an overview on actual performance of some Wi-Fi based ranging systems, which typically have an accuracy of 2.5 m to 5 m. As the Wi-Fi radio has not been designed for this purpose, various aspects and limitations must be overcome for accurate TOA measurements to the order of 1 ns. Such techniques are described in detail in the following sections, including performance estimates, and confirmation by actual measurements using a chip radio (Maxim MAX2828). While this equipment is experimental in nature, the results show that future integration into Wi-Fi chips could provide the dual roll of data communications and position location. It is also worth noting that one of the recent research focuses in Wi-Fi positioning is on the integration of such a technology with other technologies such as GNSS, RFID, or Dead-reckoning (Retscher & Fu 2009, Li *et al* 2010).

The main contributions of this paper can be summarized as follows:

1) Propose a technique for concatenating multiple Wi-Fi frequency channel data to effectively obtain a wideband signal, and derive theoretical formulas to estimate the degrading in performance associated with this technique compared with the wideband signal case.
2) Develop a procedure for the correction of local oscillator frequency offsets, and show that an accuracy of the frequency corrections of the order of 1 ppb can be achieved for mobile nodes. Previous methods described are only valid for the stationary case (anchor nodes).

The remainder of the paper is organized as follows. Section 2 provides an overview on related work. Section 3 reviews a technique of range determination using time-of-arrival (TOA) data without the need for time synchronization, with particular application to Wi-Fi radios. Section 4 describes and analyzes the performance of a method of using Wi-Fi 20 MHz channels to achieve an effective wideband channel, and hence greater time resolution for TOA measurements. Section 5 describes and analyzes a technique for very accurate frequency synchronization throughout a mesh network in an indoor NLOS propagation environment with stationary and mobile nodes. Section 6 provides some measured performance results using the methods described in previous sections. Finally, Section 7 summarizes and concludes the paper.

Overview of Related Work

Before considering the specific details of the proposed approach, this section briefly overviews some related work in the general area of Wi-Fi positioning.

1) Intel research has developed a Wi-Fi positioning system based on TOA ranging, which requires some hardware modifications to be implemented (Golden & Bateman 2007). The range is computed through performing a number of different exchanges of messages between an access point and a stationary mobile. Although some advanced signal processing techniques are used, the range root-mean-square error (RMSE) associated with 5 access points is reported as 2.66 m. Performance data for a moving node is not provided.
2) Typically in currently proposed systems, two-way TOA (equivalent to a single round-trip-time (RTT)) measurements are employed for range measurements, such as using the packet pairs DATA and ACK in the IEEE 802.11 standards. In (Llombart et al 2008) a purely software-based ranging and positioning approach is proposed and implemented by using the existing Wi-Fi hardware. Instead of using packet pairs, packet sequences (RTS, CTS, DATA and ACK) are exploited to generate multiple RTT

measurements, resulting in improved measurement accuracy, although still only 4 m.

3) The development of a WLAN channel sounder for IEEE 802.11b is reported in (Ciurana et al 2009). The sounder directly uses the physical layer characteristics of Wi-Fi systems to estimate the channel impulse response. Using a multipath propagation model and conducting a Monte-Carlo simulation, the resolution of the system is found to be nine nanoseconds, equivalent to 2.7 m.
4) A strategy is proposed in (Jemai & Kumer 2008) to reduce the position determination latency without degrading positioning accuracy. In particular a method is described to optimize the tradeoff between a short RTT response time and position update period. (Hoene & Willmann 2008) investigates the scalability issue associated with the Wi-Fi network based positioning.

None of the above is related to actual working positioning systems, and thus the actual performance in a real operating environment cannot be assessed. To investigate the potential of using Wi-Fi chips for position determination to achieve high-accuracy positioning, the techniques described in this paper have been applied to the design of an experimental positioning system called the Wireless Ad-hoc System for Positioning (WASP) (Hedley et al 2008, Sathyan et al 2011, Sharp, Yu & Hedley 2012, Sharp, Yu & Sathyan 2012). The system using a commercially available Maxim MAX2828 Wi-Fi chip in each node in the network operates in the 5.8 GHz ISM band with an effective bandwidth of 125 MHz synthesized from 20 MHz channels, and has been designed to achieve indoor positioning with an accuracy of 1 m (or better) based on a mesh network of nodes. While the above-referenced WASP papers give some information on its design and performance, key aspects such as the generation and detection of the wideband signal and the frequency synchronisation in the important case of mobile nodes have not been described previously. These topics are the main focus of this paper, providing further information on how the performance of the WASP system is achieved.

Range Measurement Overview

This section reviews the general theory of determining ranges between nodes in a network using TOA measurements. Although some of the material in this section has been described elsewhere (Hedley et al 2008, Sathyan et al 2011, Yu, Guo & Hedley 2009), the following provides more in-depth information related to the use of chip radios, and also provides the underlying theoretical framework for subsequent sections, particularly for the important practical case of a mobile node.

Transmitter to Receiver Timing Measurements

The determination of the propagation delay used for position estimation can be based on the measurement of the TOA of a radio signal at a receiver. However, the TOA measurement encompasses the total transmission delays from the transmitter to the receiver as measured relative to the clocks in the (mobile) transmitter and the receiver (stationary node or anchor node/base station), and includes the delays in the baseband hardware, the RF and IF sections of the radios, as well as the propagation delay. A block diagram of the transmission path and the associated parameters is summarized in Fig. 1. Note that transmission can be from node m to node n or in the reverse direction. In this initial analysis, it will be assumed that the clocks in the transmitter and receiver have the same frequency, but later this restriction will be removed. However, it is important to note that the clocks are not synchronised in time, so that the clocks will have a random time offset relative to an absolute time reference.

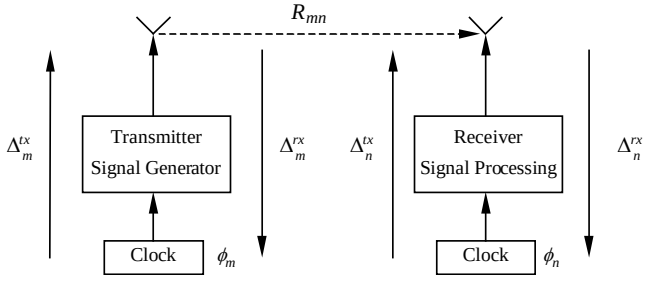

FIG. 1 BLOCK DIAGRAM SHOWING THE MAJOR COMPONENTS IN THE TRANSMISSION PATH FROM THE TRANSMITTER TO THE RECEIVER.

The transmitter baseband electronics has a clock (local oscillator) which has an (unknown) time offset relative to absolute time. Further, it is assumed that the transmissions are based on a pseudo-random noise code (or pn-code), which repeats at the code period; and that the code length is much greater than the total propagation delay, so code ambiguity does not occur. As the time measurement has a repetition period, it is appropriate for the (absolute) clock offset to be referred as a phase offset (ϕ) rather than an (unknown) absolute time offset. The baseband pn-code is used to modulate

the RF signal in the radio, which outputs the radio signal from an antenna. This process involves delays in the radio, filters, and cables, all of which are of unknown value. The total delay in the transmitter process is defined as Δ_m^{tx} for node m. Note that the delays in the radio transmitter, particularly the filters can be several hundred nanoseconds - see Fig. 2, considerably greater than the propagation delay between the nodes, and further these hardware-related delays vary over time. The reason for the variability is mostly associated with filter delay variations due to temperature and ageing effects. Further the length of the cable from the radio to the antenna can vary from node to node.

Now consider the TOA measurement in more detail. The basic time period in the transmitter and the receiver is the length of the pn-code symbol period (T_{pn}).

As the code repeats with this period, normal continuous time is not available in the receiver, so that the transmitter and receiver time is related to absolute time by

$$\phi = t \bmod T_{pn} \tag{1}$$

If the clocks are assumed to be accurately synchronised in frequency (see Section 5 for details of the frequency synchronisation), then the local time in both the transmitter (tx) and the receiver (rx) can be defined by a phase offset determined at local clock time $\phi = 0$. With reference to Fig. 1, the TOA measurement from node m to n (and ignoring measurement noise) can be expressed as

$$TOA_{mn} = \phi_m + \Delta_m^{tx} + R_{mn}/c + \Delta_n^{rx} - \phi_n \tag{2}$$

where ϕ is the clock offset phase $(0 \le \phi \le T_{pn})$ and c is the propagation speed of 0.2998 m per nanosecond.

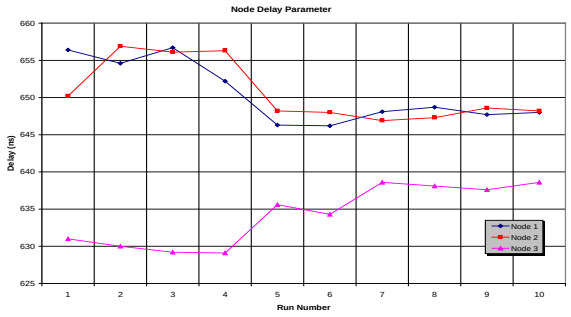

FIG. 2 MEASURED VARIATION IN THE DELAY PARAMETER FOR THREE DIFFERENT HARDWARE MODULES AS A FUNCTION OF TIME. THE DELAY DATA ARE MEASURED EVERY SECOND AND AVERAGED OVER A PERIOD OF THREE MINUTES FOR EACH RUN (RUN NUMBER) OF THE EXPERIMENT. THE PARTICULAR CHIP RADIO IS A MAXIM MAX2828.

Thus the TOA measurement involves two parameters in the transmitter and two in the receiver, but as each node has both transmit and receive functions, each unit has three parameters associated with it (the clock phase, the transmitter delay, and the receiver delay). While (2) is perfectly satisfactory for determining the TOA and further data processing, some simplification is possible by the adoption of a different time reference in each module. In particular, if the clock reference is altered so that the timing reference point is at the transmitter antenna (rather than at the baseband clock), then the TOA expression becomes

$$\begin{aligned} TOA_{mn} &= (\phi_m - \Delta_m^{tx}) + \Delta_m^{tx} + R_{mn}/c + \Delta_n^{rx} - (\phi_n - \Delta_n^{tx}) \\ &= \phi_m + R_{mn}/c + (\Delta_n^{rx} + \Delta_n^{tx}) - \phi_n = \phi_m + R_{mn}/c + \Delta_n - \phi_n \end{aligned} \tag{3}$$

Thus the TOA measurement can be expressed in terms of the clock phases in the transmitter and the receiver, the propagation delay, and the combined transmitter and receiver delays in the *receiving* unit only. As a consequence, only two parameters in each node need to be defined, namely the local clock phase and the combined radio delays. As the clock phases and radio delays are unknowns to be determined as part of the position determination process, the processing is somewhat simplified, as only two (nuisance) parameters need to be measured instead of three as in the original TOA expression. Therefore, (3) is the basic starting point in position determination.

For typical positioning systems, nodes both transmit and receive, so that it is useful to consider the TOA measurements between a pair of nodes. Thus applying (3) twice, the resulting two TOA measurements are

$$\begin{aligned} TOA_{mn} &= \phi_m + R_{mn}/c + \Delta_n - \phi_n \\ TOA_{nm} &= \phi_n + R_{nm}/c + \Delta_m - \phi_m \\ RTT_{mn} &= (TOA_{mn} + TOA_{nm})/2 = R_{mn}/c + (\Delta_m + \Delta_n)/2 \end{aligned} \tag{4}$$

where reciprocity in the propagation delay has been used (Jordan & Balmain 1968). Thus by adding two TOA measurements into a single RTT measurement, the clock phase parameters can be eliminated. If the radio delay parameters are known (preset) values, then the summed TOA measurement can be used to estimate the range. However, this typically results in low accuracy measurements due to the variability in the radio delays over time (Fig. 2), and will require individual calibration for greater accuracy. Such calibration techniques are beyond the scope of this paper, but described in (Hedley et al 2008, Sathyan et al 2011)

A key feature in the formulation described above is the use of pn-code phase rather than time. It is important to note that (4) is based on clock phase but not time, so that the two transmissions can be separated in time by a considerable amount, and thus an immediate acknowledgment of a transmission is not required. This subtle difference has important ramifications on the design of a mesh network. In a typical implementation of RTT, the receiving node replies immediately to the transmitting node. Therefore, in a network of N nodes a total on $N(N-1)$ time slots are required to avoid mutual interference; for even modestly sized mesh networks this arrangement is impractical as the update rate is low due to the large number of time slots. However, as the RTT reply transmission can be delayed in time if the measurement is based on the pn-code phase as in (4), the $N(N-1)/2$ ranges in the mesh network can be determined with only N time slots, in conjunction with the corresponding mesh network data communications. However, this method requires that the frequency offsets in the local clocks in each node is accurately compensated for, as (say) a typical local oscillator with 1-ppm accuracy would result in a RTT error of 1000 ns (300 meters) with a 1 second delay. Further, if the node moves significantly during the acknowledgment period, further timing errors will occur.

Timing Measurement Errors

The analysis in the previous section assumed ideal error-free TOA measurements, but in an actual system there will be measurement errors associated with multipath propagation and receiver noise. To minimise multipath errors, TOA measurements need to be based on the leading edge of the despread received wideband spread-spectrum signal. For the WASP system, a leading edge threshold algorithm (Sathyan et al 2011) is used, so the following discussion will be limited to that particular implementation; other leading edge algorithms (Yu, Sharp & Guo 2009, Sharp, Yu & Guo 2009) have similar characteristics.

The theoretical performance of the threshold algorithm in the presence of Gaussian noise can be calculated by assuming that the nominal pulse shape (autocorrelation function of the pn-code) is triangular, corrupted with random noise with zero mean and a STD such that the signal-to-noise ratio is $\gamma = 1/\sigma_n^2$, where the amplitude (A) of the pulse without noise is normalized to unity. The threshold for the detection of the leading edge has a nominal amplitude of $\alpha_{th}A$, or simply α_{th} in the normalized form. Although the triangular shape (with a rise-time of τ_{pulse}) is only an approximation for the bandlimited signal case, provided the threshold level is not too small $(\alpha_{th} > 0.05)$, typical shape distortions are sufficiently small (Sharp, Yu & Guo 2009) so that they have a minor effect on the TOA error due to Gaussian noise. Using techniques similar to those described in (Sharp, Yu & Guo 2009) it can be shown that the STD in the TOA error measured by the threshold algorithm is given by

$$\sigma_\varepsilon = \tau_{pulse}\sqrt{\frac{1+\alpha_{th}^2}{\gamma}} \approx \frac{\tau_{pulse}}{\sqrt{\gamma}} \qquad (5)$$

where the last approximation is made because the threshold amplitude is small in order to reduce the effects of multipath signals. This result is used later in Section 5 in the analysis of the frequency synchronization performance.

Multi-segment Concatenation

To realize the design goals outlined in Section 1 the effective time resolution of the TOA measurements must be of the order of 10 ns, or alternatively a bandwidth of at least 100 MHz. While such a bandwidth is available in the 5.8 MHz ISM band, Wi-Fi chip radios designed for IEEE 802.11a operation have a bandwidth of 20 MHz, and thus it cannot meet this design requirement. The transmission approach adopted in the WASP system is for the transmitter to sequentially scan across the ISM band one channel at a time, and for the receiver to reconstruct the wideband signal by appropriate signal processing of the logged channel data. However, as the receiver must be retuned for each channel, the data from each channel are not globally coherent (although coherent within each channel), even after an appropriate settling period for the receiver local oscillator; a coherent wideband signal is essential to perform the despreading of the wideband spread-spectrum signal. One possible method to ensure a coherent total signal is to overlap the bands in frequency, so that the overlapping frequency sections can be used to determine the differential phase between adjacent channels. In the WASP system, eight overlapping bands of bandwidth 18 MHz (total 144 MHz) are concatenated into a 125 MHz wideband signal, with about 2.5 MHz of overlap between adja-

cent channels.

Procedure for Transmitting/Reconstructing the Wideband Signal

As this paper focuses on the complications associated with the use of a chip radio rather than the details of signal processing, the following is only a summary of the procedure to generate the multi-segment signals for transmission, and the subsequent reconstruction in the receiver.

1) The spectrum of the wideband time-domain spread-spectrum signal $s_{tx}(t)$ is subdivided into overlapping segments; typically the frequency overlap required is 10-15 percent.
2) The power in each segment is normalized for equality. This lookup table of normalization constants is also known by the receiver to allow renormalization in the reconstruction process. This normalization procedure ensures constant SNR for each received segment. The inverse Fourier transform of the normalized segment spectral data is the time-domain segment data transmitted.
3) Each time-domain segment is transmitted sequentially with the appropriate RF center frequency of the Wi-Fi channel. Additionally, there is a time period between each transmission to allow the receiver to retune and stabilize the local oscillator (in phase) for reception of the next transmission.
4) The receiver calculates the spectrum of each time-domain signal segment, and uses the normalization table to correct the received spectrum of each segment to generate the wideband signal.
5) The relative phase between adjacent segments is estimated using the procedure described in detail in Section 5.2 following.
6) The differential phase data is used to rotate the phase of each segment to reconstruct the (coherent) wideband spread-spectrum signal $s_{rx}(f)$.
7) The despreading of the wideband signal is performed using the computationally efficient Fourier method. In particular the correlation diagram (correlogram) is generated by the operation

$$C(\tau) = \mathrm{FFT}^{-1}\left(\mathrm{FFT}(s_{rx}(t))\mathrm{FFT}(s_{tx}(t))^*\right) \tag{6}$$

Note that the Fourier transforms of the received segment signals required in step (4) are used in the calculation of the correlogram, so little additional computations are required to calculate the differential phases. Also note that the Fourier transform of the transmitted signal is invariant, and thus the results are stored as a data table in the receiver which uses the wideband time-domain correlogram to estimate the TOA of the signal.

Recovering the Differential Phase

Consider two segments of overlapping complex spectral data. The receiver output can be represented as

$$\begin{aligned} &\text{Segment 1}: A_1 S(f) e^{j\phi_1} \\ &\text{Segment 2}: A_2 S(f) e^{j\phi_2} \end{aligned} \tag{7}$$

where the (random) phases ϕ_1, ϕ_2 are unknown, but the relative amplitudes are known by the receiver from the normalization table described previously. To recover the differential phase while reducing the effects of noise, the following frequency-domain correlation is performed

$$C = \int_0^{\Delta f} \left(A_1 S(f) e^{j\phi_1}\right)\left(A_2 S(f) e^{j\phi_2}\right)^* df = A e^{j(\phi_1 - \phi_2)} E_{seg} \tag{8a}$$

where $A = A_1 A_2$, $E_{seg} = \int_0^{\Delta f} |S(f)|^2 df$ is the energy in the overlapping segment, and receiver noise has been ignored. As the segment energy is a real number, the differential phase can be recovered by

$$\phi_1 - \phi_2 = \Delta\phi_{12} = \arg(C) \tag{8b}$$

While the above analog correlation process can recover the differential phase, in practice the receiver output will include noise, and the signals are in a sampled form. Thus from (8a) with processing of sampled data the correlator output will be

$$C = A e^{j(\phi_1 - \phi_2)} \sum_{i=1}^{N_{ovr}} \left(\left(\hat{S}_1^i\right)\left(\hat{S}_2^i\right)^*\right) = A e^{j(\phi_1 - \phi_2)} \sum_{i=1}^{N_{ovr}} \hat{C}_i = A e^{j(\phi_1 - \phi_2)} \hat{C} \tag{9a}$$

where the ith sample of the digital noisy complex spectra is given by

$$\begin{aligned} &\text{Segment 1}: \hat{S}_1^i = \left(S_R^i + n_{11}^i\right) + j\left(S_I^i + n_{12}^i\right) \\ &\text{Segment 2}: \hat{S}_2^i = \left(S_R^i + n_{21}^i\right) + j\left(S_I^i + n_{22}^i\right) \end{aligned} \tag{9b}$$

where the random noise n has the statistical properties $E[n] = 0$ and $\mathrm{var}[n] = \sigma_n^2$, and the four noise com-

ponents in (9b) are statistically independent. Unlike the integration in (8a), the summation in (9a) is complex, and thus performing (8b) using (9a) will result in an error in the differential phase estimate. Now consider properties of the real and imaginary components of $\hat{S}^i$. The expected value of the real component of ith sample is $E\left[\mathrm{Re}\left(\hat{C}_i\right)\right]=\left(S_R^i\right)^2+\left(S_I^i\right)^2=P_s^i$ (the signal power of the ith sample), so the summation over the N_{ovr} samples in the overlapping region is proportional to the energy in the overlapping segment as in (8a). The corresponding variance is

$$\mathrm{var}\left[\mathrm{Re}\left(\hat{C}_i\right)\right]=E\left[\mathrm{Re}\left(\hat{C}_i^{\,2}\right)\right]-E\left[\mathrm{Re}\left(\hat{C}_i\right)\right]^2=2\sigma_n^2\left[P_s^{i\,2}+\sigma_n^2\right] \quad (10)$$

Since the transmitted signals are pseudo-random, the real and imaginary spectral components are quasi-random and statistically independent, with means $E[S_R]=E[S_I]=0$ and variances $\mathrm{var}[S_R]=\mathrm{var}[S_I]=\sigma_s^2$. Applying these conditions to the N_{ovr} overlapping samples in the segment gives

$$\begin{aligned}E\left[\mathrm{Re}\left(\hat{C}\right)\right]&=2N_{ovr}\sigma_s^2\\ \mathrm{var}\left[\mathrm{Re}\left(\hat{C}\right)\right]&=4N_{ovr}\sigma_s^2\sigma_n^2\left(1+1/2\gamma_s\right)\end{aligned} \quad (11)$$

where the pre-correlation segment spectrum SNR is $\gamma_s=\sigma_s^2/\sigma_n^2$, as the (normalized) segment power is $2\sigma_s^2$ and the noise power is $2\sigma_n^2$. From (11) the output SNR (γ) for the real component of $\hat{C}$ is

$$\gamma=\frac{\left(2N_{ovr}\sigma_s^2\right)^2}{4N_{ovr}\sigma_s^2\sigma_n^2\left(1+1/2\gamma_s\right)}=\frac{\sigma_s^2N_{ovr}}{\sigma_n^2\left(1+1/2\gamma_s\right)}=\frac{N_{ovr}}{1+1/2\gamma_s}\gamma_s \quad (12)$$

Therefore this correlation has a process gain of $N_{ovr}/\left(1+1/2\gamma_s\right)\approx N_{ovr}$, where the last approximation is a consequence of the segment pre-correlation SNR typically being much greater than unity. A similar analysis for the imaginary component of $\hat{C}$ gives

$$\begin{aligned}E\left[\mathrm{Im}\left(\hat{C}\right)\right]&=0\\ \mathrm{var}\left[\mathrm{Im}\left(\hat{C}\right)\right]&=4N_{ovr}\sigma_s^2\sigma_n^2\left(1+1/2\gamma_s\right)\approx 4N_{ovr}\sigma_s^2\sigma_n^2\end{aligned} \quad (13)$$

The imaginary component of $\hat{C}$ is responsible for errors in estimating the differential phase as defined by (8b). As the phase error in radians is approximately the imaginary component divided by the real component (for small phase errors), combining the first equation in (11) with the second equation in (13) gives the STD of the phase error (in radians) approximately as

$$\sigma[\Delta\phi]\approx\frac{\sqrt{4N_{ovr}\sigma_s^2\sigma_n^2\left(1+1/2\gamma_s\right)}}{2N_{ovr}\sigma_s^2}=\sqrt{\frac{1+1/2\gamma_s}{\gamma_s}}\frac{1}{\sqrt{N_{ovr}}} \quad (14)$$

In deriving (14), as the mean of real part of $\hat{C}$ is much greater than its STD, the small variation in the real part is ignored. Thus given a particular segment SNR, the STD of the differential phase error decreases inversely as the square root of the length of the overlapping segment. However, increasing the overlapped part of the segment reduces the transmission efficiency, so in practice this is limited to a small fraction of the total segment length. Consider a typical numerical example, with parameters similar to the WASP system. To ensure adequate performance the pre-correlation signal SNR is $\gamma_s\geq 0$ dB, and the length of the overlap is $N_{ovr}=64$ samples out of a total segment length of 512 samples. Applying (14) gives $\sigma[\Delta\phi]\leq 0.153$ radians. While this phase error is quite small, the variance of the differential phase error (relative to the first segment) increases proportional to the segment number, so the relative phase error in the last segment can be quite large. The cumulative effect of these errors is considered in the next section.

Reconstructed Signal Correlation Performance

Having determined the statistics of the differential phase error between adjoining segments, the overall effect on the wideband time-domain correlation of the spread-spectrum signal is now estimated. Although the wideband spectrum power varies across the band (maximum in the center and approaching zero at the edges), the power in each transmitted segment is normalized so that the transmitted power in each segment is similar, and hence the SNR in each segment is approximately the same. As a consequence, from (14) the STD of the phase error in each segment will be similar. Further, the contribution of each segment to the overall time-domain correlation (without phase errors) will also be approximately similar. Thus using the first segment as a phase reference, the relative effect of the differential phase errors on the correlator output is given by

$$\Gamma_c=1+\sum_{s=1}^{N_{seg}-1}e^{j\Phi_s} \quad (15a)$$

where

$$\Phi_s = \sum_{n=1}^{s} \Delta\phi_n \tag{15b}$$

is the summation of phase errors accumulated in a random-walk fashion across the reconstructed received time-domain signal. However, the magnitude of (15a) would involve a square-root operation, making statistical calculations difficult. Thus as an alternative, the statistics of the magnitude-squared (power) is analysed, so that with N_{seg} segments the relative power is

$$\begin{aligned}\Gamma_{cc} = \Gamma_c \Gamma_c^{*} &= \left(1 + \sum_{s=1}^{N_{seg}-1} e^{j\Phi_s}\right)\left(1 + \sum_{s=1}^{N_{seg}-1} e^{j\Phi_s}\right)^{*} \\ &= N_{seg} + 2\sum_{s=1}^{N_{seg}-1} \cos(\Phi_s) + 2\sum_{s=2}^{N_{seg}-2}\sum_{t=s+1}^{N_{seg}-1} \cos(\Phi_s - \Phi_t)\end{aligned} \tag{16}$$

To further simplify the statistical calculations associated with (16), as the phase terms are generally relatively small (see numerical calculation in Section 4.2) the cosines in (16) are approximated by means of the truncated Taylor series $\cos x \approx 1 - x^2/2$. Thus the expectation (mean) of (16) can be approximated by

$$E[\Gamma_{cc}] = N_{seg}^{\,2} - \sum_{s=1}^{N_{seg}-1} E[\Phi_s^{\,2}] - \sum_{s=2}^{N_{seg}-2}\sum_{t=s+1}^{N_{seg}-1} E[(\Phi_s - \Phi_t)^2] \tag{17}$$

By applying (15b) and assuming the differential phase errors of each segment pair have the same variance and are statistically independent (due to the random phase associated with the frequency scanning process by the receiver) the expectations in (17) become

$$\begin{aligned}\sum_{s=1}^{N_{seg}-1} E[\Phi_s^{\,2}] &= \sum_{s=1}^{N_{seg}-1} E\left[\left(\sum_{n=1}^{s}\Delta\phi_n\right)^2\right] = \sum_{s=1}^{N_{seg}-1}\sum_{n=1}^{s} E[\Delta\phi_n^{\,2}] \\ &= \left[\frac{N_{seg}(N_{seg}-1)}{2}\right]\sigma_{\Delta\phi}^{\,2} \\ \sum_{s=2}^{N_{seg}-2}\sum_{t=s+1}^{N_{seg}-1} E[(\Phi_s - \Phi_t)^2] &= \sum_{s=2}^{N_{seg}-2}\sum_{t=s+1}^{N_{seg}-1} E\left[\left(\sum_{n=1}^{s}\Delta\phi_n\right)^2\right] \\ &= \left[\frac{N_{seg}(N_{seg}-1)(N_{seg}-2)}{6}\right]\sigma_{\Delta\phi}^{\,2}\end{aligned} \tag{18}$$

where $\sigma_{\Delta\phi}$ is given by (14). Substituting these results into (17) and normalizing $E[\Gamma_{cc}]$ by the zero phase error value N_{seg}^2 gives the expected relative correlator output power as

$$E[\hat{\Gamma}_{cc}] / N_{seg}^2 = 1 - \left[\frac{(N_{seg}^{\,2}-1)}{6N_{seg}}\right]\sigma_{\Delta\phi}^{\,2} \approx 1 - \frac{N_{seg}\sigma_{\Delta\phi}^{\,2}}{6} \tag{19}$$

Equation (19) gives the loss in the process gain due to the phase errors. For example, from the example in Section 4.2 with $\sigma_{\Delta\phi} = 0.153$, applying (19) gives a trivial loss of 0.13 dB. Fig. 3 shows the loss in Process Gain as a function of the number of samples in the overlap and the input SNR. For minimal impact on the performance, the number of samples should be greater than 50 and the input SNR greater than –3 dB, which is realized by the WASP system.

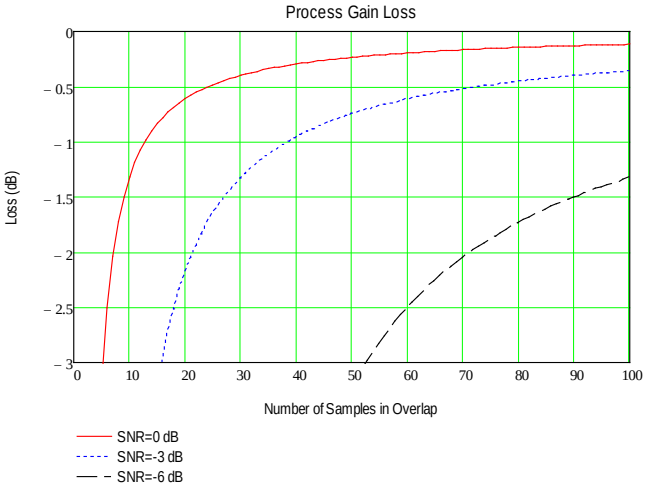

FIG. 3 VARIATION IN THE PROCESS GAIN LOSS AS A FUNCTION OF THE NUMBER OF SAMPLES IN THE OVERLAP AND THE INPUT SNR (γ_s).

Frequency Offset Estimation

The analysis in Section 3 assumed perfect frequency synchronization throughout the mesh network. This section describes a frequency synchronization technique, and estimates the accuracy of the synchronization process as well as its effect on TOA measurements, for both stationary (anchor nodes) and moving nodes.

Accurate frequency synchronisation in the mesh network is required to ensure that clock drifts between transmitting and receiving a reply do not result in RTT measurement errors. For example, if the two TOA measurements associated with the RTT measurement are one second apart in time, then a differential drift of 1 ppb in the clocks represents a RTT measurement error of 1 ns. As typical low-cost oscillators have frequency errors of the order of 1-10 ppm, the system must provide a frequency synchronisation correction to reduce this initial error by at least a factor of 1000.

Fig. 4 shows the measured variation in differential frequency between two oscillators over a long period of time in a temperature-controlled (air-conditioned) office environment. It is assumed in the following analy-

sis that over short periods of time (up to a few minutes) the differential frequency is considered constant. However, over longer periods of time the variation is of the order of 20 ppb, so that differential frequency tracking is essential if an overall differential frequency error not greater than 1 ppb is to be met.

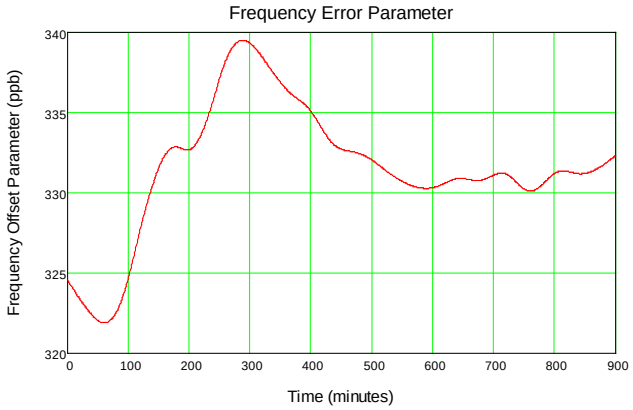

FIG. 4 MEASURED DIFFERENTIAL FREQUENCY PARAMETER BETWEEN TWO OSCILLATORS OF NOMINAL ACCURACY OF 1 PPM. THE FREQUENCY DIFFERENTIAL OVER THE 15 HOURS VARIES BY ABOUT ±10 PPB. THE DATA IN THIS GRAPH HAVE BEEN SMOOTHED TO REMOVE SHORT-TERM MEASUREMENT NOISE.

Frequency Synchronization Procedure

The basic concept to estimate the relative drift between two oscillators has been described in (Yu, Guo & Hedley 2009), but the following analysis provides more information on the process as well as analysis of the stationary case, and describes a new method for the practically important moving node case.

The basic method to estimate the differential frequency is to determine the rate of change in the TOA between measurements separated in time. The TOA estimate from (3) can be modified to account for a linear drift in the clock over a time period (t) as measured by the local clock. Defining the linear clock phase function as

$$\Phi(t,\alpha) = \mathrm{mod}\left(\phi^0 + \alpha t, T_{pn}\right) \qquad (20a)$$

the resulting TOA estimate as a function of time is given by

$$TOA_{mn}(t) = \Phi(t,\alpha_m) + \left(R_{mn} + \delta R_{mn}\right)/c + \Delta_n - \Phi(t,\alpha_n) + T_{noise} \qquad (20b)$$

where at t=0 the clock phases are their nominal values ϕ^0 based on their local clock, and the phases are assumed to change linearly over subsequent time. The time (t) in (20a) for the frequency offset estimation will be over many pn-code periods up to (say) one minute, and thus it is implied from (20a) that ϕ^0 is a constant at the start of transmissions over many pn-code periods if there is no frequency error; in practice for the method to work the transmissions must always commence at the start of a pn-code period, or $\mathrm{mod}(t, T_{pn}) = 0$, where t measured by the local clock. Additionally in (20b), a range error has been added due to multipath propagation, plus a random measurement noise T_{noise} (with a zero mean). The mod function in (20a) complicates analysis, as the phase function has a sawtooth shape (Yu, Guo & Hedley 2009) with a sudden change of T_{pn} at a period of T_{pn}/α. As α is a small number, this sudden change in the TOA will occur infrequently, and as this change is of known value, the measured TOA data as a function of time can be easily corrected by "unwrapping" the raw measurements (either up or down depending on the sign of the drift). With this correction, the mod operation in (20a) can be ignored in the analysis of performance, so if the two nodes are stationary and the multipath environment is static, then (20b) can be written in the form of a linear equation over time with additive noise, namely

$$TOA_{mn}(t) = \beta_{mn} + \alpha_{mn} t + T_{noise} \qquad (21)$$

where $\alpha_{mn} = \alpha_m - \alpha_n$ and $\beta_{mn} = \left(\phi_m^0 - \phi_n^0\right) + \left(R_{mn} + \delta R_{mn}\right)/c + \Delta_n$, a constant, at least over the frequency estimation period (T) which is typically of the order of 10 seconds. If a series of TOA measurements is performed over time (typically with a constant update period of (say) 1 second), then a linear regression analysis can be performed to determine the differential frequency drift parameter α_{mn}. Note that the value of the constant parameter β is not required in determining the differential frequency parameter, so that range measurement errors due to multipath do not affect the estimation of differential frequency. However, the random component will result in errors in the estimate of the differential frequency parameter; and this uncertainty can be calculated using the estimated STD in the TOA as given by (5) in Section 3.2. After unwrapping, the regression analysis on (21) results in an estimate of the STD in the differential frequency parameter as

$$\sigma(\alpha_{mn}) = \sqrt{\frac{12}{M}}\frac{\sigma_\varepsilon}{T} \qquad (22)$$

where σ_ε , the STD of the TOA measurement, is given by (5), T is the total period of the sampling, and M is the number of measurements $(M >> 1)$. Applying (5) with a (low) SNR of 20 dB, and 11 measurements with an update period of 1 second (so T=10 seconds), (22) results in an (upper) estimated STD in the differential frequency parameter of 0.15 ns per second (or 0.15 ppb). Thus if the nodes are stationary the frequency offset can be readily estimated to a precision that results in trivial errors in the TOA, even if there are multipath errors in the TOA measurements.

The above procedure is satisfactory for static nodes where the changes in the TOA as a function of time can be interpreted as a consequence of a differential frequency between the two nodes. However, if one node is mobile, the changes in TOA can also be due to movement of the mobile node so that in this case the measurement of the differential frequency by the above method is not possible.

Estimation of Range Error due to Motion

Before analysing the problem of determining the frequency offset parameter for a moving node, consider the range estimation performance for moving nodes without frequency offsets. The RTT measurement procedure consists of the mobile node transmitting and stationary nodes within radio range replying. Each node in the mesh network has an assigned time slot for transmissions, which incorporates both the spread-spectrum signals used for TOA measurement and data transmission. For example, the WASP system in (Sharp, Yu & Sathyan 2012) has $N_s = 60$ time slots of 10 ms period (T_s), so the position update period (T_u) is 0.6 second. The delay in the reply depends on the time slots assigned to the mobile unit and the replying nodes, so a delay of p time slot periods will be in the range $T_s \ldots T_u$. From (4) and ignoring any frequency synchronization error, the RTT will be

$$RTT_{m,n} = \frac{1}{2}\left[(\Delta_m + \Delta_n) + \frac{(2R_{mn} + \delta R_{mn})_0 + (D + \delta R_{nm})_p}{c} \right] + T_{noise} \tag{23}$$

where D is the effective differential distance due to movement by the mobile over the interval from the time of transmitting to receiving a reply, and is given by $D = vpT_s \cos\theta$, where v is the speed, p is the slot delay parameter, and θ is the angle between the velocity and range vectors. For the WASP example above the maximum distance travelled in the update period is 0.9 m, where it is assumed that the mobile unit is attached to a person walking at a speed of 1.5 m/s. As the actual distance will vary dependent on the geometry and slot numbers, this distance can be considered as quasi-random, so that from (23) the range error due to motion is given by

$$\varepsilon_v = \frac{1}{2}\left[vpT_s \cos\theta + (\delta R_0 + \delta R_p) \right] + cT_{noise} \tag{24}$$

which has three statistically independent components, one associated with the movement of the mobile node, the second associated with multipath propagation, and the third associated with receiver noise. Now consider the statistical properties of the motion-related random process. The slot delay parameter p can be considered as having a statistical uniform distribution $[-N_s/2, N_s/2]$ with a mean delay of $T_u/2$, and the angle between velocity and range vectors can be considered as statistical uniform distribution over $[-\pi, \pi]$, where it is assumed that the replying nodes "surround" the mobile node in a statistically uniform manner. Thus averaging over all anchor nodes and positions in the coverage area the expected value of the range error associated with motion is

$$E[\varepsilon_v] = \frac{vT_s}{2} E[p\cos\theta] = \frac{vT_s}{2} E[p] E[\cos\theta] = 0 \tag{25a}$$

as both expectations in the last expression in (25a) are zero. Therefore on average the motion of the mobile does not result in any range error measured at a point in time delayed by $T_u/2$ relative to the initial transmission by the mobile node. As the unbiased range error reference time will vary with each node pair, for maximum accuracy in position determination a velocity vector correction should be applied. In most cases this complication is unnecessary. Similarly the variance of the motion-related error can be calculated to be

$$\mathrm{var}[\varepsilon_v] = \left(\frac{vT_s}{2}\right)^2 E[p^2] E[(\cos\theta)^2] = \frac{1}{2}\left[\frac{vT_s}{2}\right]^2 \left[\frac{N_s^2}{12}\right] = \frac{(vT_u)^2}{96} \tag{25b}$$

For example, when using (25b), the numerical values in the above WASP example give the STD in the range as 0.092 m. In an indoor environment the random multipath component of the range error STD (for the WASP system data, see Table 1) is typically of the order of 1 m for static range measurements averaged over a large coverage area (Sharp, Yu & Hedley 2012,

Sharp, Yu & Sathyan 2012). However, if the mobile unit moves a distance greater than about a wavelength in a NLOS propagation environment, the two TOA errors associated with the RTT measurement will be largely uncorrelated due to the random Rayleigh scattering of the radio signal. For the WASP case with a wavelength of about 5 cm, and for the above walking case, the distance travelled in one slot period is 1.5 cm, so nearly all of the slot delays will result in uncorrelated measurements. Thus from (23) with two statistically independent random variables δR, the effect of the averaging two TOA measurements reduces the range error STD by about a factor of $\sqrt{2}$. Note that this applies only to the random component, but bias errors will be essentially constant over small distances, and thus the frequency synchronization process is not affected. However, it is shown in (Sharp, Yu & Sathyan 2012) that mounting a mobile unit on the body of a person causes shadowing effects which results in increased GDOP, so the overall positional accuracy (product of GDOP and ranging error STD) may be worse than that with stationary base stations, despite the improved ranging error STD.

Frequency Synchronization for Mobile Nodes

While the frequency synchronization described in Section 5.1 is a simple procedure involving just TOA measurements between two stationary nodes, a modified method is required when one of the nodes is moving. One possible method to determine this motion status is by means of processing the data from an accelerometer in the mobile node. In particular, if the measured acceleration "noise" is below a threshold, then the node is deemed to be stationary, and the differential frequency parameter is calculated as described in Section 5.1. When the accelerometer "noise" is above the threshold, a previously measured (when stationary) differential frequency parameter value could be used. However, from Fig. 4, even under ideal conditions, the differential frequency parameter will vary slowly. If (say) the maximum allowable drift is 1 ppb, it is suggested from Fig. 4 that the period in which the previously estimated value can be used is at most several minutes. The length of time will depend on the quality of the oscillator, so if this method is to be used, good quality (and expensive) oscillators are required. As the design goal is for cheap hardware, such a strategy is not ideal due to its unreliability when the period of motion without stopping exceeds a few minutes. Thus an alternative method of estimating the frequency offset parameter in nodes which are in motion is highly desirable.

Before describing the method, it is useful to further refine the method of defining the offset frequency parameter in each node. In the method described in Section 5.1 only a differential parameter between two nodes is required, but for the moving node case, the estimation of the frequency offset parameter for all neighbouring nodes in the mesh network is required, which will be explained below. As only relative frequency synchronization is required, not absolute synchronization, it is appropriate for one node in the mesh network to act as the network frequency reference, and all other nodes are synchronized to this reference node. By definition, this node now is deemed to have a zero offset frequency parameter, namely $\alpha_{ref} = 0$. Further, as all stationary nodes which communicate with the reference node can determine the differential offset frequency relative to the reference node, these nodes also can determine their frequency offset parameter, which can be transmitted in communications with other nodes. Thus by this procedure, with communications throughout the mesh network, all stationary nodes (but as yet not moving nodes) can update in real-time their frequency offset parameter, and transmit this information to other nearby nodes. This procedure will result in a slow increase in the frequency offset errors as the number of hops from the reference node increases, so that with N_{hop} hops, the STD in the frequency offset parameter will be $\sqrt{N_{hop}}\sigma(\alpha)$, where $\sigma(\alpha)$ is given by (22). However, this reduction in the accuracy can be readily compensated for by increasing the measurement time T in (22), so the accuracy estimate of 0.15 ppb in Section 5.1 can be maintained in the multi-hop case. Furthermore, the frequency offset correction process used in correcting raw RTT measurements still only uses the relative offset between adjacent pairs of nodes, so the range error analysis in Section 5.2 remains valid for multi-hop stationary nodes.

Having established the frequency offset parameter in each stationary node, the next requirement is to establish this parameter for mobile nodes in real-time whilst in motion. The proposed method is similar to position determination using pseudorange data, whereby a range offset common to all measurements is determined as well as the (x, y) position. Because of this similarity with pseudorange least-squares (LS)

positioning described elsewhere (Yu, Sharp & Guo 2009), only a summary of the details will be given here. From (4) and (23), the range measurement between a mobile (m) and stationary node (n) can be expressed as

$$R_{mn} = \left[cRTT_{mn} - \frac{c\alpha_n(t_2 - t_1)}{2} - c\left(\frac{\Delta_m + \Delta_n}{2}\right)\right] + \frac{c\alpha_m(t_2 - t_1)}{2} - \left[\left(\frac{\delta R^1_{mn} + \delta R^2_{nm}}{2}\right) + \frac{D_{mn}}{2} + cT_{noise}\right] \quad (26)$$

where t_1 is the time of the transmission from the mobile to the stationary node, t_2 is the time of the reply, and D_{mn} is the effective distance as defined in Section 5.2. The first term in square brackets in (26) is either a measurement or a known value, while the second term is only a function of the mobile node (independent of the stationary nodes) with the only unknown the sought-after mobile node frequency offset parameter α_m, and the last term is a random variable, which in Section 5.2 is shown to be dominated by the range errors associated with the indoor multipath environment.

The scattering of radio signals indoors is complex and depends on the details of the indoor environment, so theoretical calculations are difficult. However, experimental measurements (Alavi & Pahlavan 2006, Bellusci et al 2008, Gentile & Kik 2006, Alsindi et al 2009) and WASP range error data (Sharp, Yu & Hedley 2012, Sharp, Yu & Sathyan 2012) show that indoor NLOS ranging errors have a bias error which increases approximately linearly with range, and a random component which is largely independent of range, provided a small percentage (typically less than 10 percent) of large range errors are excluded; this exclusion is justified as they will be rejected in the position determination process (Yu, Sharp & Guo 2009, Sathyan et al 2011). Thus the indoors NLOS range error model assumed for the following theoretical analysis is

$$\Delta R = (\delta R_0 + \lambda R) + \varepsilon_R = \beta_R + \varepsilon_R \quad (27)$$

where the term in brackets is the linear bias model (β_R), and ε_R is a random component with zero mean. Thus if a LS analysis over all nodes in radio range of the mobile node is performed to determine the four unknowns $(\alpha_m, \beta_R, x, y)$, the last three of which in this case are nuisance variables, then an estimate of the frequency offset parameter can be obtained.

Using model (27) and (25b), (26), an analytical LS analysis (similar to that in (Yu, Sharp & Guo 2009, Sharp, Yu & Hedley 2012) shows that $E[\alpha_m] = 0$, and the STD in the frequency offset parameter of the mobile node is approximately given by

$$\sigma(\alpha_m) \approx \sqrt{\frac{3}{N_R + 5/9N_R}}\frac{4}{cT_u}\sigma_{\Delta R} \approx \sqrt{\frac{24}{N_R}}\left(\frac{\sigma_r}{cT_u}\right) \quad (28)$$

where $\sigma_{\Delta R}{}^2 = \frac{\sigma_r^2}{2} + \frac{(\lambda R_{\max})^2}{18} + \frac{(vT_u)^2}{96}$, N_R is the number of stationary nodes in range, and $R_{\max}$ is the maximum radio range. In (28) it is assumed that the range measurements to the stationary nodes are statistically independent (because of the random indoor NLOS scattering), and that these nodes "surround" the mobile node in a statistically uniform manner, as described in (Sharp, Yu & Hedley 2012). Notice that the STD is approximately inversely proportional to the square-root of the number of nodes in range, and also inversely proportional to the update period; these relationships are similar to the stationary case given by (22).

The simulation results of the frequency offset estimation process are shown in Fig. 5. The simulation is based on a mobile unit moving along a circular path with parameters as defined in the caption text for Fig. 5.

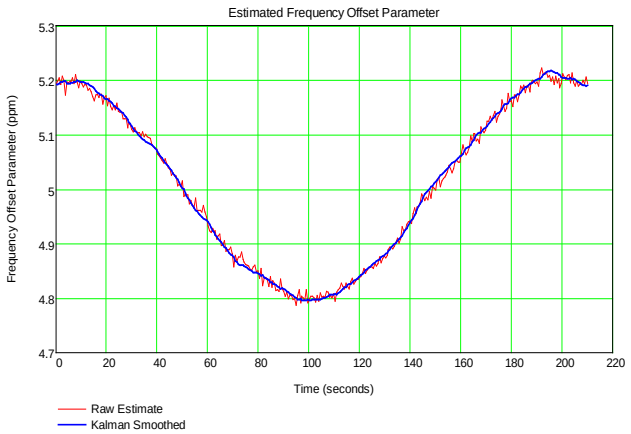

FIG. 5 SIMULATED PERFORMANCE OF ESTIMATING THE FREQUENCY OFFSET PARAMETER FOR A NODE MOVING AT A SPEED OF 1.5 M/S ON A CIRCULAR PATH OF RADIUS 25 M WITH AN UPDATE PERIOD OF 0.6 SECONDS. THE COVERAGE AREA IS 100 M SQUARE, WITH 44 NODES UNIFORMLY RANDOMLY DISTRIBUTED (BUT WITH A MINIMUM SEPARATION OF 7.5 M), OF WHICH (ON AVERAGE) 18 ARE WITHIN RADIO RANGE. THE RANGE ERROR MODEL PARAMETERS ARE $\lambda = 0.03$, $\sigma_r = 1$ m, WITH A MAXIMUM RADIO RANGE OF 40 M.

The frequency offset is represented by a mean of 5 ppm plus a sinusoidal component with amplitude 200 ppb and a period of 200 seconds, similar to those assumed in the simulation in (Yu, Guo & Hedley 2009). This variation is not intended to model actual frequency variations, but to demonstrate the ability to dynamically track quite rapid variations. The mesh network parameters chosen are typical of the deployment of the WASP system in an indoor office-type environment. Fig. 5 shows both the raw estimate of the frequency offset parameter, as well as the Kalman filtered smoothed version. The raw data has a mean error in the frequency offset of 1.6 ppb with a STD of 8.1 ppb, compared with the analytical estimate from (28) of 7.8 ppb. The filtering is based on a Singer g-h-k Kalman filter (Brookner 1998) for tracking a target whose dynamics have a random acceleration with a exponential autocorrelation function with a time constant of 200 seconds. The STD of the Kalman filtered data is 4.8 ppb. As described in Section 5.2, the RTT reply period (T) is a pseudo-random variable (uniform distribution in the range 0 to 0.6 second in this case), so the associated STD in the range is $c\sigma(\alpha)T/\sqrt{12} = 0.26$ m. Assuming that the range bias errors are corrected for, so that only the random range errors ($\sigma_r = 1$ m in this case) remain, then the random effects in the estimation of the frequency offset parameter will result in the effective STD in the random range error increasing to $\sqrt{1^2 + 0.26^2} = 1.03$ m. Thus the effect on ranging accuracy by errors associated with the determination of the frequency offset parameter for a moving node is insignificant

Measured Performance Results

The methods described in the previous sections have been implemented in the WASP positioning system, so that testing of the theory is possible through measurements. However, as the overall performance is the integrated sum of the individual subsystems, such as the signal concatenation and frequency synchronization processes which are the focus of the methods and analysis described in this paper, the performance of these individual subsystems cannot be analysed in details. However, it is confirmed that the ranging performance meeting expectations is indicative that the subsystems also perform within specifications.

The WASP performance data are summarized in Table 1, and are listed in chronological order. The data include both range (Δr) and position errors (ε), mean and median statistics, static and dynamic measurements, and LOS/NLOS propagation environments. The data for the first four cases in Table 1 are in the indicated referenced paper, while the final case is reported here for the first time. Note also that the number of nodes increases from the initial 9 to the final 46 nodes; and that the corresponding area covered increases from 225 m2 to 10,000 m2. The final example is for the WASP system deployed in a complex of buildings, much as would be expected in a commercial deployment. Although there are a wide variety of data presented in Table 1, the general conclusion is that LOS performance (range and position) is 15 cm or better, while NLOS performance (in a building) is generally better than 1 m.

The static LOS measurement errors at high SNR (about 50 dB) are dominated by errors associated with the wideband reconstruction and frequency synchronization subsystems. The 15 cm STD (or 0.5 ns) range measurement noise can be attributed to "reconstruction noise" associated with the wideband signal concatenation process, and as such represents the lower limit in possible ranging performance. This lower limit in ranging also places a lower limit on the accuracy of the frequency synchronization process. Applying (22) with M=11 and T=10 seconds yields a trivial frequency error STD of 0.055 ppb. Even at the typical lower operating SNR of 30 dB, the estimate frequency STD would be 0.55 ppb. In these cases, it is clear that frequency synchronization errors will not be a problem. The NLOS measurements listed in Table 1 have ranging errors of the order of 0.5-1 m. In this case, the indoor multipath propagation environment is the dominant factor, rather than the performance of the analog radio and its associated signal processing. These WASP performance data are much better than other reported results (as summarized in Section 2) by at least a factor of 5, which is about the factor (125 MHz to the 20 MHz Wi-fi channel ratio) of the wideband reconstruction process. This result suggests that the reconstruction process described in Section 4 is effective in a multipath environment, with the improvement factor close to the bandwidth enhancement factor. Ultimately, performance in the NLOS indoor environment is limited by available bandwidth in the ISM bands, rather than the signal reconstruction process.

TABLE 1. SUMMARY OF PERFORMANCE DATA OF WASP SYSTEM AS REPORTED IN THE INDICATED PAPER.

Paper	LOS Δr_{rms}	NLOS Δr_{rms}	Nodes	Area, $\bar{\mathbf{d}}$	Static NLOS $\bar{\varepsilon}_{pos}$	Static NLOS $\tilde{\varepsilon}_{pos}$	Dyn NLOS $\bar{\varepsilon}_{pos}$	Dyn LOS $\tilde{\varepsilon}_{pos}$
Hedley *et al*, 2008	15 cm		9	225 m², 5.0 m		49 cm		
Sathyan *et al*, 2011	15 cm		9	225 m², 5 m	48-61 cm			7 cm (3)
Sharp, Yu & Sathyan, 2012			29	2100 m², 8.5 m	48 cm		76 cm	
Sharp, Yu & Hedley, 2012		108 cm	36	2100 m², 7.6 m	46 cm (1),70-100 cm (2)			
		94 cm	46	10000 m², 14.7 m		65 cm		

(1) Core locations in building, (2) Positions at the edge of buildings, (3) Based on two mobile units 0.7 m apart on a bike in a velodrome - measures differential position error only. The "~" symbol signifies the median.

Conclusion

This paper investigated the application of IEEE 802.11/Wi-Fi analog chip-radios to positioning systems. Because of the desire for cheap implementation in commercial applications, it is proposed that the Wi-Fi chip-radios used for data communications are also used for radiolocation applications in indoor environments. Achieving the desired sub-meter ranging accuracy with this type of radio is challenging, as the design of these chip radios is aimed at data communications rather than radiolocation. To achieve the goal of accurate radiolocation, two main areas where innovative design is required have been identified, namely achieving an effective wide bandwidth, and frequency synchronization in a mesh network with mobile nodes, all in a radio-hostile indoor multipath propagation environment. By using commercially available analog chip-radios and appropriate signal processing techniques, it has been shown that indoor ranging accuracy of about 1 m can be obtained, and that when applied in a mesh network, positioning accuracy of 0.5 m can be obtained without the need to adopt ultra-wide bandwidths and the associated high frequency (and power hungry) electronics, or complicated timing synchronization schemes. Current generation Wi-Fi chips have close integration of both the analog radio and digital signal processing functions into a single chip, so that the methods used in the WASP system could not be readily adopted with such chips. However, it is suggested that by adding further specialized signal processing hardware, a chip with both Wi-Fi data communications and accurate radio location functionality could be developed without much difficulty.

REFERENCES

Alavi, Bardia, and Kaveh Pahlavan. "Modeling of the TOA-based distance measure error using UWB indoor radio measurements." IEEE Communications Letters 10(2006): 275-277.

Alsindi, Nayef A., Bardia Alavi, and Kaveh Pahlavan. "Measurement and modelling of ultra wideband TOA-based ranging in indoor multipath environments." IEEE Trans. Vehicular Technology 58(2009): 1046-1058.

Bahl, Paramvir, and Venkata N. Padmanabhan. "RADAR: an in-building RF-based user location and tracking system." In Proc. of IEEE Conf. Computer Communications (INFOCOM), 2000, 775-784.

Bellusci, Giovanni, Gerard J.M. Janssen, Junlin Yan, and Christian C.J.M. Tiberius. "Model of distance and bandwidth dependency of TOA-based UWB ranging error." in Proc. of IEEE Int. Conf. on Ultra-Wideband, 2008, 193-196.

Brookner, Eli. Tracking and Kalman Filtering Made Easy, John Wiley and Sons Inc., 1998.

Ciurana, M., F. Barcelo-Arroyo, and M. Llombart. "Improving the performance of TOA over wireless systems to track mobile targets." in Proc. IEEE Int. Conf. on Communications Workshops, Jun. 2009, 1-6.

FCC Part 15 (Title 47 of the Code of Federal Regulations transmission rules, Part 15 - Radio Frequency Devices, subpart C - Intentional Radiators).

Fontana, Robert J. "Recent system applications of short-pulse ultra-wideband (UWB) technology." IEEE Trans. Microwave Theory and Technology 52(2004): 2087-2104.

Fontana, Robert J., Edward Richley and Joann Barney. "Commercialization of an ultra wideband precision asset location system." In Proc. of IEEE Conf. UWB systems and Technologies, 2003, 369-373.

Frank V. Diggelen. A-GPS: GPS, GNSS and SBAS. Artech

House, 2009.

Gentile, Camillo, and Alfred Kik. "An evaluation of ultra wideband technology for indoor ranging." in Proc. of IEEE Globecom, 2006, 1-6.

Ghassemzadeh1, S., L. Greenstein, A. Kavcic, T. Sveinsson, and V. Tarokh. "UWB Indoor Delay Profile Model for Residential and Commercial Environments." IEEE Trans. on Vehicular Technology 54(2005): 1235-1244.

Golden, Stuard A., and Steve S. Bateman. "Sensor measurements for Wi-Fi location with emphasis on time-of-arrival ranging." IEEE Trans. on Mobile Computing 6(2007): 1185-1198.

Hedley, Mark, David Humphrey and Phil Ho. "System and algorithms for accurate indoor tracking using low-cost hardware." In Proc. of IEEE/IOA Position, Location and Navigation Symposium, May 2008, 633-640.

Hoene, Christian, and Jorg Willmann. "Four-way TOA and software-based trilateration of IEEE 802.11 devices." in Proc. IEEE Personal, Indoor and Mobile Radio Communications (PIMRC), Cannes, Sep. 2008, 1-6.

Jardak, Nabil, and Nel Samama. "Indoor positioning based on GPS-repeaters: performance enhancement using an open code loop architecture." IEEE Trans. on Aerospace and Electronic Systems 45(2009): 147-159.

Jemai, Jaouhar, and Thomas K. Kurner. "Broadband WLAN channel sounder for IEEE 802.11b." IEEE Trans. on Vehicular Technology 57(2008): 3381-3392.

Jordan, Edward C., and Keith G. Balmain. Electromagnetic Waves and Radiating Systems. Second Edition, Prentice-Hall, 1968.

Li, Binghao, Andrew G. Dempster, and Chris Rizos. "Positioning in environments where GPS fails." In Proc. of FIG Congress, Sydney, Australia, April 2010

Llombart, M., M. Ciurana, and F. Barcelo-Arroyo. "On the scalability of a novel WLAN positioning system based on time of arrival measurements." in Proc. of Workshop on Positioning, Navigation and Communication (WPNC), Mar. 2008, 15-21.

Mourad, Farah, Hichem Snoussi, and Cedric Richard. "Interval-based localization using RSSI comparison in MANETs." IEEE Trans. on Aerospace and Electronic Systems 47(2011): 2897-2910.

Retscher, Guenther, and Qing Fu. "Integration of RFID, GNSS and DR for ubiquitous positioning in pedestrian navigation." Journal of Global Positioning Systems 6(2007): 56-64.

Roy, Sumit, Jeff R. Foerster, V. Srinivasa Somayazulu, and Dave G. Leeper. "Ultrawideband Radio Design: The Promise of High-Speed, Short-Range Wireless Connectivity." Proc. of the IEEE 92(2004): 295-311.

Samper, Jaizki M., Roc B. Perez, and Juan M. Lagunilla. GPS and Galileo: Dual RF Front-end receiver and Design, Fabrication and Test. McGraw Hill, 2009.

Sathyan, Thuraiappah, David Humphrey, and Mark Hedley. "WASP: A System and Algorithms for Accurate Radio Localization using Low-cost Hardware." IEEE Trans. Society, Man and Cybernetics - Part C 41 (2011): 211-222.

Sharp, Ian, Kegen Yu, and Y. Jay Guo. "Peak and leading edge detection for time-of-arrival estimation in band-limited positioning systems." IET Communications 3(2009): 1616-1627.

Sharp, Ian, Kegen Yu, and Mark Hedley. "On the GDOP and Accuracy for Indoor Positioning." IEEE Transactions on Aerospace and Electronic Systems 48(2012): 2032-2051.

Sharp, Ian, Kegen Yu, and Thuraiappah Sathyan. "Positional Accuracy Measurement and Error Modeling for Mobile Tracking." IEEE Transactions on Mobile Computing 11(2012): 1021-1032.

Yu, Kegen, Y. Jay Guo, and Mark Hedley. "TOA-Based Distributed Localization with Unknown Internal Delays and Clock Frequency Offsets in Wireless Sensor Networks." IET Signal Processing 3(2009): 106-118.

Yu, Kegen, Ian Sharp, and Y. Jay Guo. Ground-Based Wireless Positioning. Wiley and IEEE Press, June 2009.

Ian Sharp is a Senior Consultant on wireless positioning systems. He has over thirty years of engineering experience in radio systems. His initial involvement in positioning technology was in aviation, and later in the 1980s with the Interscan microwave landing system (MLS). In the later 1980s to the early 1990s, Ian was the R&D manager for the Quiktrak covert vehicle tracking system. This system is now commercially operating world-wide. From mid 1990s to 2007, Ian worked at the CSIRO mainly on developing experimental radio systems. He is the inventor and architect designer of CSIRO's precision location system (PLS) for outdoor sporting applications, and later the initial development of the Wireless Ad-hoc System for Positioning (WASP) indoor positioning system. Ian holds a number of patents related to positioning technology. He is a co-author of the

book: Ground-Based Wireless Positioning (Wiley and IEEE Press, 2009).

Kegen Yu received the PhD degree in electrical engineering from the University of Sydney in 2003. He initially worked as Associate Engineer at Jiangxi Geological and Mineral Bureau and Associate Lecturer and later Lecturer in the Department of Industrial Automation at Nanchang University. Subsequently, Dr. Yu was Post-doc Research Fellow at the Centre for Wireless Communications, University of Oulu; Research Scientist at the CSIRO ICT Centre; and Research Fellow in the Department of Electronic Engineering at Macquarie University. Currently, he is Senior Research Fellow at the Australian Centre for Space Engineering Research and the School of Surveying & Geospatial Engineering, University of New South Wales. Dr. Yu is currently on the editorial board of EURASIP Journal on Advances in Signal Processing, IEEE Transactions on Aerospace and Electronic Systems, and IEEE Transactions on Vehicular Technology. He is Lead Guest Editor for the special issue of Physical Communication on 'Indoor Navigation and Tracking' and for the special issue of EURASIP Journal on Advances in Signal Processing on 'GNSS Remote Sensing'. He is Senior Member of IEEE and Adjunct Professor at Macquarie University. He co-authored a book (Ground-Based Wireless Positioning, Wiley and IEEE Press; a Chinese version of the book is also available) and book chapters in three books published by Wiley. He also authored or co-authored about 30 refereed journal papers and over 30 refereed conference papers. His current research interests include ground-based and GNSS-based positioning and GNSS remote sensing.